Numerical simulation of the 2011 Tohoku tsunami: Comparison with field observations and sensitivity to model parameters

Stephan T. Grilli[1], Jeffrey C. Harris[1], Tayebeh Tajalibakhsh[1], James T. Kirby[2], Fengyan Shi[2]
Timothy L. Masterlark[3], and Christodoulos Kyriakopoulos[1]

(1) Department of Ocean Engineering, University of Rhode Island, Narragansett, RI, USA
(2) Center for Applied Coastal Research, University of Delaware, Newark, Delaware, USA
(3) Department of Geological Sciences, The University of Alabama (UoA), Tuscaloosa, Alabama, USA
(4) Instituto Nazionale di Geofisica e Vulcanologia, Rome, Italy

ABSTRACT

The March 11, 2011 M9 Tohoku-Oki Earthquake, which is believed to be the largest event recorded in Japan history, created a major tsunami that caused numerous deaths and enormous destruction on the nearby Honshu coast. Various tsunami sources were developed for this event, based on inverting seismic or GPS data, often using very simple underlying fault models (e.g., Okada, 1985). Tsunami simulations with such sources can predict deep water and far-field observations quite well, but coastal impact is not as well predicted, being over- or under-estimated at many locations. In this work, we developed a new tsunami source, similarly based on inverting onshore and offshore geodetic (GPS) data, but using 3D Finite Element Models (FEM) that simulate elastic dislocations along the plate boundary interface separating the stiff subducting Pacific Plate, and relatively weak forearc and volcanic arc of the overriding Eurasian plate. Due in part to the simulated weak forearc materials, such sources produce significant shallow slip along the updip portion of the rupture near the trench (several tens of meters).

We assess the accuracy of the new approach by comparing numerical simulations to observations of the tsunami far- and near-field coastal impact, using: (i) one of the standard seismic inversion sources, which we found provided the best prediction of tsunami near-field impact in our model (UCSB; Shao et al. (2011)); and (ii) the new FEM source. Specifically, we compare numerical results to DART buoy, GPS tide gage, and inundation/runup measurements. Numerical simulations are performed using the fully nonlinear and dispersive Boussinesq wave model FUNWAVE-TVD, which is parallelized and available in Cartesian or spherical coordinates. We use a series of nested model grids, with varying resolution (down to 250 m nearshore) and size, and assess effects on results of the latter and of model physics (such as when including dispersion or not). We also assess effects of triggering the various tsunami sources in the propagation model: (i) either at once as a hot start, or with the spatio-temporal sequence derived from seismic inversion; and (ii) as a specified surface elevation or as a more realistic time and space-varying bottom boundary condition (in the latter case, we compute the initial tsunami generation up to 300 s using the non-hydrostatic model NHWAVE).

Although additional refinements are expected in the near future, results based on the current FEM sources better explain near field observations at DART and GPS buoys near Japan, and measured tsunami inundation, while they simulate observations at distant DART buoys as well or better than the UCSB source.

KEYWORDS: Tsunami source modeling; Tsunami propagation modeling; Boussinesq model; Wave dispersion effects.

INTRODUCTION

On March 11th, 2011, at 2:46 pm JST, a magnitude $M_w = 9.0$ earthquake struck near the northeastern coast of Japan (37°49' N, 143°03' E; Fig. 1), with substantial slip at fairly shallow depths (about 10-20 km), causing large seafloor motions that triggered very high tsunami waves, perhaps the largest in Japan's recorded history. The main earthquake shocks lasted for 3-4 minutes and, owing to the proximity of the epicenter to shore, the first significant waves reached Japan only 10 minutes after the event started, thus allowing for very little warning time. The tsunami caused extensive destruction along the coast of the Tohoku region, between 35° - 43° N. Post-tsunami surveys reported maximum of runups and inundation depths values in the 20-40 m range, mostly between 37.7° - 40.2° N where the Miyagi and Iwate Prefectures are located (The 2011 Tohoku Earthquake Tsunami Joint Survey Group, 2011; Mori et al., 2011a). The largest runups occurred in the north, along the Sanriku/Ria coast (north of 37° N), which has a very complex topography that amplifies tsunami impact. By contrast, areas located directly south, which mostly consist of plains, were less impacted. As a result of the tsunami, nearly 16,000 people lost their lives and 4,000 were reported missing; many were injured and millions more were affected by the lack of water and food, electricity, and transportation (IOC/UNESCO, 2011).

Within one hour of the event, when the tsunami reached the nearest DART buoys (Deep-water Assessment and Reporting of Tsunami network; Gonzalez et al. (1998); Fig. 1), propagation models of the anticipated far-field impact caused sufficient concern to trigger evacuations and warnings in many distant areas across the Pacific Ocean. Large impact was predicted as far as Chile, where waves were expected to arrive af-
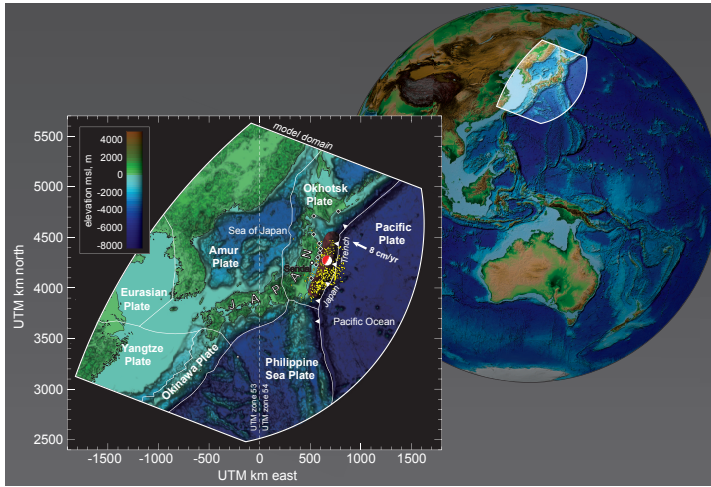
Fig. 1: M9 2011 Tohoku earthquake seismotechtonics (rupture zone marked by red polygon). Large symbol is the epicenter; yellow dots show M > 4 aftershocks (11 March 06 May 2011). The Pacific-Okhotsk plate convergence is about 8 cm/yr. Black diamonds mark coastal GPS wave buoys (Yamazaki et al., 2011a).

ter more than 20 h of propagation. In the meantime, through a chain of failures of coastal protections and back-up power systems caused by the earthquake and the tsunami inundation, the core of one of the reactors at the Fukushima Dai-Ichi nuclear power plant (near $37° 25'$ N) started melting, eventually causing explosions that released large doses of radiation, forcing a complete evacuation in the days following the event of all people living within tens of kilometers of the power plant that will likely last for many decades.

The earthquake ruptured the boundary separating the subducting Pacific Plate from the overriding Okhotsk Plate; this segment of the plate boundary intersects the seafloor at the Japan Trench (Fig. 1), where it dips about $10°$ to a down-dip distance of about 100 km from the trench. The rupture area, 150 km east of Sendai, Japan, extends a few hundred km in the along strike direction, offshore of the Prefectures of Aomori, Miyagi, and Fukushima. At the latitude of the earthquake, the Pacific Plate moves approximately westwards with respect to the Okhotsk Plate at a rate of 8 cm/yr (DeMets et al., 1994) (Fig. 1). The focal mechanisms reported by Harvard CMT, the U.S. Geological Survey (USGS), and the Earthquake Research Institute at the University of Tokyo, all indicated that the earthquake was predominantly thrust with a moment more than $M_o \simeq 4.0 \times 10^{22}$ N.m and a variety of seismic, geodetic, and tsunami genesis studies concluded that the magnitude was indeed $M_w = 9.0$ (e.g., Ide et al. (2011)). Some geodetic inversion models (e.g., Ozawa et al. (2011); Pollitz et al. (2011)) suggest that the peak slip may have exceeded 30-35 m in some areas, while some seismic inversion models suggest over 50-60 m of maximum slip (e.g., Ammon et al. (2011); Shao et al. (2011); Lay et al. (2011a)). Owing to the small dip angle, such large slip values caused very large uplift of the seafloor, likely reaching well over 10 m in a large central area of the tsunami source (Fig. 1).

MODELING OF THE TOHOKU-OKI CO-SEISMIC SOURCE

Since the Tohoku event, a large variety of seismic models of the earthquake have been proposed. These were usually based on inverting seismic and/or geodetic data, using the Okada (1985) model, which assumes a superposition of planar dislocations (i.e., finite faults) embedded in homogeneous elastic half-spaces (HEHS), or a similarly idealized source

model of the subduction zone (e.g., Dziewonski's 1981 spherical layered PREM seismological model; see, e.g., Ammon et al. (2011); Geospatial Information Authority of Japan (2011); Pollitz et al. (2011); Ozawa et al. (2011); Shao et al. (2011)). One of these seismic inversion sources, referred to as UCSB (Shao et al., 2011), will be used in this study (see details below).
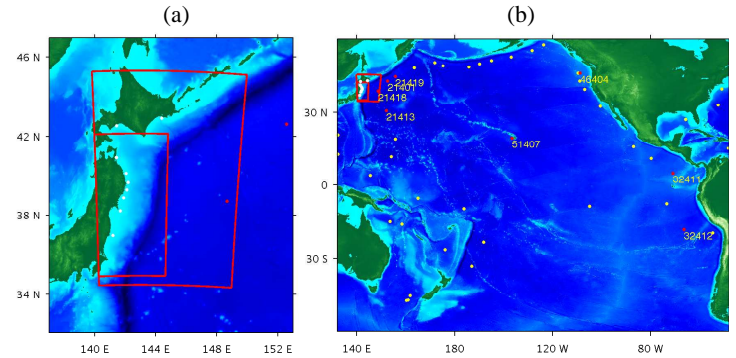

Fig. 2: Computational domains for FUNWAVE-TVD simulations: (a) near-field (regional 1000 m and coastal 250 m, large/small red boxes) Cartesian grid (also for NHWAVE); and (b) far-field (Pacific basin scale) 4' spherical grid, with marked location of 18 DART buoys (yellow/red dots). White dots in (a) indicate locations of the GPS buoys of Fig. 1

In the present work, to better account for the actual geometry of the Japan trench and its forearc, as well as inhomogeneities in material properties in the subduction zone (e.g., weaker forearc and stiffer subducting plate materials), we developed and used our own source, based on a more comprehensive and detailed Finite Element Modeling (FEM) (Masterlark, 2003) of the subduction zone near Japan. An earlier implementation of this approach was successfully applied to the 2004 M9 Sumatra-Andaman earthquake (Masterlark and Hughes, 2008). This new tsunami source (referred to as University of Alabama; UA) was developed by inverting onshore and offshore geodetic data but, rather than using Okada's idealized HEHS solution, it used 3D FEMs to simulate elastic dislocations along the plate boundary interface separating the stiff subducting Pacific Plate, and relatively weak forearc and volcanic arc of the overriding Eurasian plate. Details are given below.

Another aspect of co-seismic sources that affects tsunami simulations in a propagation model is whether one triggers the maximum seafloor deformation at once, as a hot start in the model, for the entire source area, or triggers sub-areas of the source as a time sequences that mimics the actual earthquake event. Such a time sequence can be obtained as a result of seismic inversion methods. In this event, seismic inversion models (e.g., Harvard CMT) show that the main earthquake lasted for 3-4 minutes, during which tsunami waves may have propagated a large distance towards Japan. Hence, in the present case, it is important to trigger waves as a function of time and resolve interferences (constructive or destructive) that may have resulted. The sensitivity of tsunami generation to this timing aspect will be studied in the present work. Additionally, we will study the sensitivity of results to the way the tsunami is initially specified in the propagation model: (i) either as a free surface elevation with no initial velocity (as it is customary to do in most studies owing to the near incompressibility of water and small rise times); (ii) or as a more realistic time dependent bottom boundary condition (in this case a different type of model, NHWAVE, that allows for such a boundary condition will first be used during 300 s, before moving results into a long wave propagation model; this is detailed later).
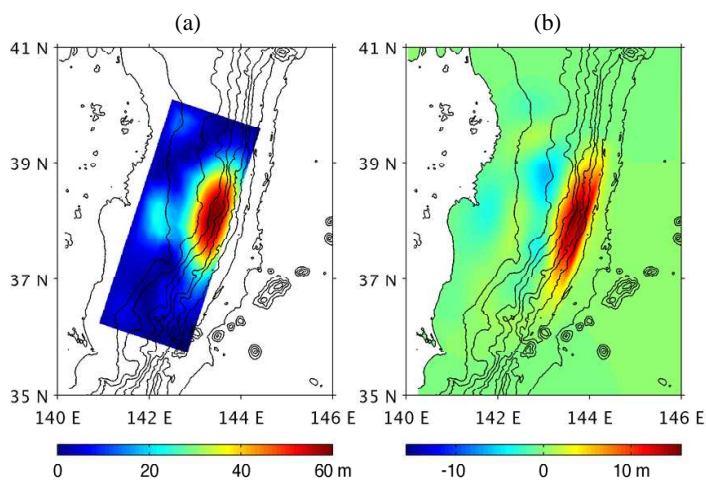
Fig. 3: UCSB source (Shao et al., 2011): (a) Source area and maximum slip distribution; and (b) vertical seafloor displacement.

UCSB source

The source we denote as UCSB is based on the slip history derived by Shao et al. (2011) using tele-seismic body and surface seismic waves. It assumes, the earthquake epicenter was located at $38.10°$ N and $142.86°$ E, and the seismic moment was $M_o = 5.84 \times 10^{22}$ N.m, for a dip angle of $10°$ and a strike angle of $198°$. Fig. 3 shows the maximum slip distribution obtained for this source, as well as the corresponding maximum vertical seafloor displacement.

UA source

This source is developed by simulating the deformation of the Tohoku earthquake (as measured at GPS stations; Fig. 4, a) using FEMs of the subduction zone, rather than idealized semi-analytical solutions. Such FEMs simulate an assembly of dislocation surfaces embedded in a 3D elastic domain, and are constructed with Abaqus (2009); they share the general geometry, mesh and distribution of material properties presented by Masterlark and Hughes (2008) and Hughes et al. (2010).

The FEM domain is configured to simulate net deformation along a rupture surface having the along-strike curvature of the Japan Trench and a dip of about $12°$. The dimensions of the curved rupture are about 750 km$\times 200$ km along-strike and downdip, respectively. This rupture surface is partitioned into 98 dislocation patches. The domain is partitioned into six regions representing the different elastic properties of the forearc, volcanic arc, shallow and deep backarc, oceanic crust, and mantle. The distribution of slip along the rupture is calibrated via least-squares inverse methods, by assimilating three-component geodetic data from 521 onshore GPS stations (GEONET of Japan, processed by the ARIA team at JPL/Caltech; ftp://sideshow.jpl.nasa.gov/pub/usrs/ARIA) and 5 offshore stations (Sato et al., 2011), that characterize the nearfield coseismic deformation of the M9 Tohoku earthquake. Details of the FEM models set-up and computational methods can be found in Grilli et al. (2012).

The maximum magnitude of slip for this solution is about 51 m, and the solution corresponds to a moment magnitude of $M_w = 8.8$, which is perhaps slightly on the lower side (Fig. 4, b). For this reason, we also investigated an alternative solution that corresponds to a moment magnitude of $M_w = 9.0$ (in better agreement with seismogenic studies of the event) by reducing the damping coefficient, which relaxes the smoothing

constraints and consequently improves the fit to the data. The maximum slip magnitude for this alternative solution is 85 m. Predictions of geodetic data are excellent for both models.

MODELING OF THE TOHOKU-OKI TSUNAMI

Early forecasts of the Tohoku tsunami far-field impact, such as issued by NOAA's Pacific Tsunami Warning Center, were not based on real-time tsunami modeling, but instead on the SIFT (Short-term Inundation Forecast for Tsunamis) database; i.e., these were developed through a tsunami data inversion technique and site-specific inundation forecasts (Gica et al., 2008). Detailed modeling of the event, both earthquake and tsunami generation, and of tsunami propagation and near- and far-field impacts, which is the object of the present work, was tackled in the months following the event. Such work first involves, as discussed above, developing a relevant tsunami source that accounts for local geological and tectonic processes as well as observed seismic and geodetic (i.e, directly measured seafloor and land deformation) data. Using such a source together with sufficiently accurate and resolved bathymetric and topographic data, numerical models of tsunami generation, propagation, and coastal impact can be run, whose results are then compared to available field data (e.g., tide gage and deep water DART buoys, runup and inundation measurements). Modeling refinements may follow and, once a reasonable agreement between simulations and observations is achieved, numerical results can be used to better understand tsunami processes that unfolded during the event. Improved design and construction methods for tsunami mitigation techniques can finally be suggested. Along this line, for instance, Yamazaki et al. (2011b) studied the effects of the Tohoku tsunami on Hawaii, using two of the early proposed finite-source models obtained from seismic and geodetic inversions (Lay et al., 2011b), and applying their "Non hydrostatic Evolution of Ocean Wave" (NE-OWAVE) tsunami propagation model. They used forward modeling of tsunami records at the 4 DART buoys located nearest Japan to refine the location of the main fault slip. They then modeled far-field tsunami propagation and compared model results to DART buoy measurements made throughout the Pacific, GPS buoy and wave gage data near the Japanese coast, and tide gage and runup measurements in Hawaii. They reported a reasonable agreement at most locations between simulations and observations, although they needed to introduce a time shift in the computed time series at the farthest distant locations.
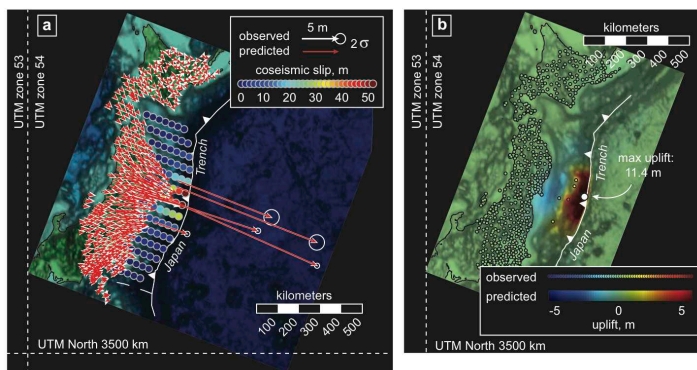

Fig. 4: UA source. (a) Coseismic slip and horizontal deformation. (b) Vertical deformation. The observed vertical displacement (colored circles) are well predicted by the calibrated FEM. Note the substantial uplift near the trench (up to 11.4 m).

Summary of tsunami generation and propagation models

Large co-seismic tsunamis have usually been simulated using (non-dispersive) Nonlinear Shallow Water (NSW) wave equation models (e.g., Kowalik and Murty (1993)). By contrast, the more dispersive landslide tsunamis have been simulated with Boussinesq models (BM), or similar models, which are nonlinear and dispersive (Watts et al., 2003; Day et al., 2005; Tappin et al., 2008). More recently, however, dispersive models such as BMs have also been increasingly used to simulate co-seismic tsunamis (Grilli et al., 2007, 2010; Ioualalen et al., 2007; Karlsson et al., 2009). Although dispersive effects may not always be significant in long tsunami wave trains, when they are called for, BM equations feature the more extended physics required for simulating such effects; Ioualalen et al. (2007), for instance, showed differences in the computed elevation of leading waves, for the 2004 Indian Ocean tsunami event near Thailand, of up to 30% when simulating the tsunami using a BM with or without the dispersive terms.

We model the Tohoku event using the BM model FUNWAVE, which was initially developed and validated for coastal wave dynamics problems (Wei et al., 1995; Chen et al., 2000, 2003; Kennedy et al., 2000); this model was later used to perform tsunami case studies (e.g., Ioualalen et al. (2007)). In its most recent implementation, FUNWAVE-TVD, in Cartesian (Shi et al., 2012) or spherical coordinates with Coriolis effects (Kirby et al., 2009, 2012), the code uses a TVD shock-tracking algorithm that more accurately simulates wave breaking and inundation. Earlier work shows that the numerical diffusion resulting form the TVD scheme yields an accurate representation of wave height decay in the surfzone (Shi et al., 2012). For tsunamis, FUNWAVE-TVD has been validated against a large set of analytical, laboratory, and field benchmarks (Tehranirad et al., 2011) as part of the development of tsunami hazard maps for the US East Coast. Because of their more complex equations, BMs are typically more computationally demanding than NSW models. For this reason, an optimized MPI parallel implementation of FUNWAVE-TVD was developed, which has highly scalable algorithms with a typical acceleration of computations of more than 90% the number of cores in a computer cluster (Shi et al., 2012). This makes it possible running the model over large ocean basin-scale grids, with a sufficiently fine resolution. Present results will show that dispersive effects are not significant in the near-field for the type of tsunami sources used to date. However, as these sources are refined (both in space and time) to include more complex geological processes (e.g., sub-faults and splay faults), one will increasingly have to model the superposition and interactions of shorter and hence more dispersive waves, which requires using models that simulate this type of physics (such as BMs).

To specify and study effects of time-dependent tsunami sources triggered by transient motion of the seafloor (which is not a feature of FUNWAVE-TVD), the non-hydrostatic model NHWAVE developed by Ma et al. (2012) will be used to compute the initial tsunami generation (up to $t = 300$ s). NHWAVE provides a numerical solution of the three-dimensional Navier Stokes equations for incompressible flows, in a σ coordinate framework (typically with 3 levels), but with the simplifying assumption of a single-valued water surface displacement. Ma et al. (2012) have validated the model performance for landslide tsunami generation by comparing to the highly dispersive laboratory data presented by Enet and Grilli (2007). FUNWAVE-TVD or NHWAVE are initialized with either the USCB or the new UA source. Once generated, we simulate the near-field tsunami propagation from the source to the Japan coast in FUNWAVE-TVD's Cartesian implementation and the far-field tsunami propagation from the source to distant locations in the Pacific Ocean in its spherical implementation. Fig. 2 shows the ocean-basin scale domain (with 4' arc mesh (b); spanning $132°$ E to $68°$ W and $60°$ S to $60°$ N) used for the far-field propagation computations, and the more finely resolved regional grid (with 1000 m mesh (a) large; 800 by 1200 km), encompassing both the earthquake source and the Japan coastline, used for computing near-field tsunami impact. Finally, runup and inundation simulations are done in a smaller coastal grid (with 250 m mesh (a) small). Earth's sphericity is corrected in Cartesian coordinates with a transverse secant Mercator projection with its origin located at ($39°$ N, $143°$ E). This transformation leads to small grid distortions, which are deemed negligible.

In all (FUNWAVE or NHWAVE) simulations, free-slip (wall) boundary conditions are applied on solid lateral boundaries. To prevent non-physical reflection from these boundaries, sponge layers are specified over a number of grid cells to absorb outgoing waves (inside of the outer domain boundary marked in Fig. 2), for which damping terms are activated in the model equations. For the Pacific grid, sponge layers are 100 km thick along all lateral boundaries and, in the regional grid, they are 50 km thick in the north and south ends of the domain, and 200 km thick in the east. Finally, in the 250 m coastal grids, sponge layers are 50 km thick along the north, east and south boundaries.

FIELD DATA

Many tsunami observations were made during and after the event. For comparison with model simulations and validations, we will use: (i) deep water DART buoy measurements of surface elevation (Lay et al., 2011b); (ii) nearshore GPS buoy or tide gauge measurements of surface elevation (Yamazaki et al., 2011a); and (iii) onshore runup and inundation height (The 2011 Tohoku Earthquake Tsunami Joint Survey Group, 2011; Mori et al., 2011a,b).

The latter data was recorded at more than 5,300 individual locations during post-event surveys conducted by a large international team of scientists, along a 2,000 km stretch of the Japanese. Inundation heights were obtained from watermarks on trees, walls, and buildings, and detided for the time of tsunami impact. Run-up heights were derived from the maximum extent of debris deposits and water marks. DART buoy data is routinely collected in 15 s to 15 minute intervals, depending on the level of alert. When the passage of a tsunami has been identified at a particular buoy (after the DART network has been put on alert), average surface elevation data is transmitted every 15 s during the initial few minutes, followed by 60 s intervals (Gonzalez et al., 1998). To obtain the tsunami signal, this data first needed to be filtered to remove the tidal signal (Butterworth filter) and it was then interpolated to get equal intervals of 15 s. DART buoys used here are labeled in Fig. 2. A series of moored GPS-mounted buoys from the NOWPHAS (Nationwide Ocean Wave information network for Ports and HArbourS; http://nowphas.mlit.go.jp/infoeng.html) moored near the Japan coast (in water depth of 100 to 300 m and at a distance of 10 to 20 km from the coastline; Fig. 1) resisted the large tsunami waves. After applying a low-pass filtering with a moving average technique, these provided time series of surface elevation.

Bathymetric and topographic data used in modeling was compounded from: the 1' arc resolution ETOPO1 database, the 500 m resolution J-EGG500 bathymetry (JODC-Expert Grid data for Geography) along the Japanese coastline, and the 1 arc-second ASTER topographic data. In deep water, only ETOPO1 data was used while for the regional/coastal grids, the other (finer) data sources were used whenever available. Data from various sources was linearly interpolated.
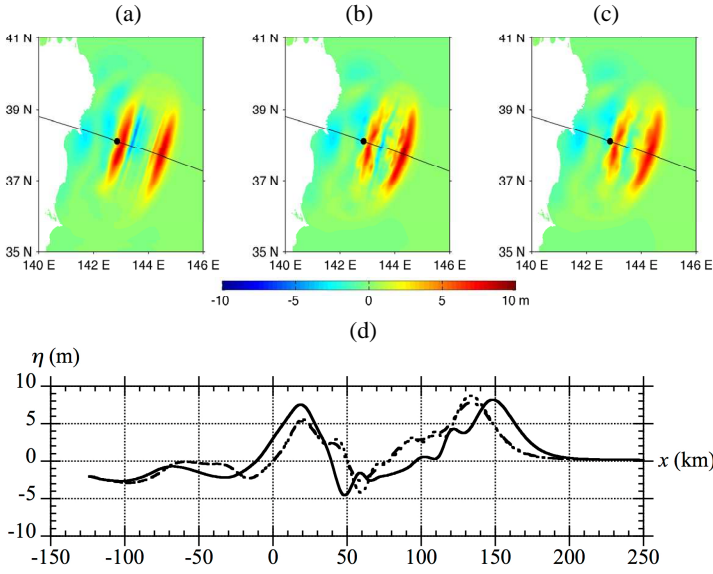
(a) (b) (c)

(d)

Fig. 5: Sensitivity of initial tsunami elevation computed at $t = 300$ s to the initialization method, for the UCSB co-seismic source : (a) instantaneous triggering on the free surface in FUNWAVE-TVD, with maximum seafloor displacement; (b) time-varying triggering on the free surface in FUNWAVE-TVD, with instantaneous seafloor displacement; and (c) time-varying seafloor displacement specified as a boundary condition in NHWAVE. Black lines indicate locations of transect used in (d), and the black dot is the origin of the axis in the latter figure. (d) transect in results for method : (—) (a); (− − −) (b); (− - −) (c).

RESULTS

As indicated, we simulate the propagation of the Tohoku 2011 tsunami across the Pacific Ocean, and its coastal transformations, runup and inundation along the Japanese coastline, in a series of computational domains (Fig. 2). All numerical simulations begin with 300 s of computations of the initial tsunami waveform in the 500 by 800 km, 1000 m resolution, regional grid, in which we first study the sensitivity of results to whether the co-seismic tsunami sources are triggered at once or in a time sequence in the propagation model. In the latter case, we also verify whether it is relevant to linearly superimpose non-moving free surface elevations, when triggering large tsunami waves in a time sequence.

Results at 300 s (or 5 mins.) are then interpolated, through a one-way coupling, from the regional grid onto one of two FUNWAVE-TVD grids (Table 1): either (i) directly on the 4' arc spherical grid for far-field transpacific simulations; or (ii) following an additional 10 min. of propagation in the 1000 m FUNWAVE grid, onto the 250 m resolution coastal Cartesian grid (in order to both get the westward propagating waves to fully enter the 250 m grid and separate these from the eastward propagating wave), to perform all near-field simulations. The latter include computations of time series at GPS tide buoys as well as computations of run-up and inundation along the coast.

Result sensitivity to initialization method

Three types of initializations are tested and compared in the regional grid for the UCSB co-seismic source shown in Fig. 3: (1) a hot start of FUNWAVE-TVD as a free surface elevation without initial velocity, by either (a) specifying the maximum seafloor vertical displacement at once (e.g., such as in Fig. 3, or (b) as a time-dependent triggering; (2) as a time-dependent bottom boundary condition in NHWAVE. Fig. 5 shows the computed free surface elevations at $t = 300$ s and a transect in

those, for these three cases. Significant differences can be seen, in both surface elevation and wavelength, between the instantaneous method (1a) and the two time-dependent methods (1b,2). Smaller differences can then be observed between the latter two methods, with the time-triggering in NHWAVE resulting in slightly reduced maximum (positive or negative) elevations and in waveforms with less higher-frequency oscillations than for the time-triggering in FUNWAVE-TVD. This might be due to the adjustment of the solution kinematics to the non-physical superposition of free surface increments with no initial velocity. Overall, these results justify using the 3rd more accurate and realistic method to compute the initial tsunami waveform, which will be done in all the following computations.
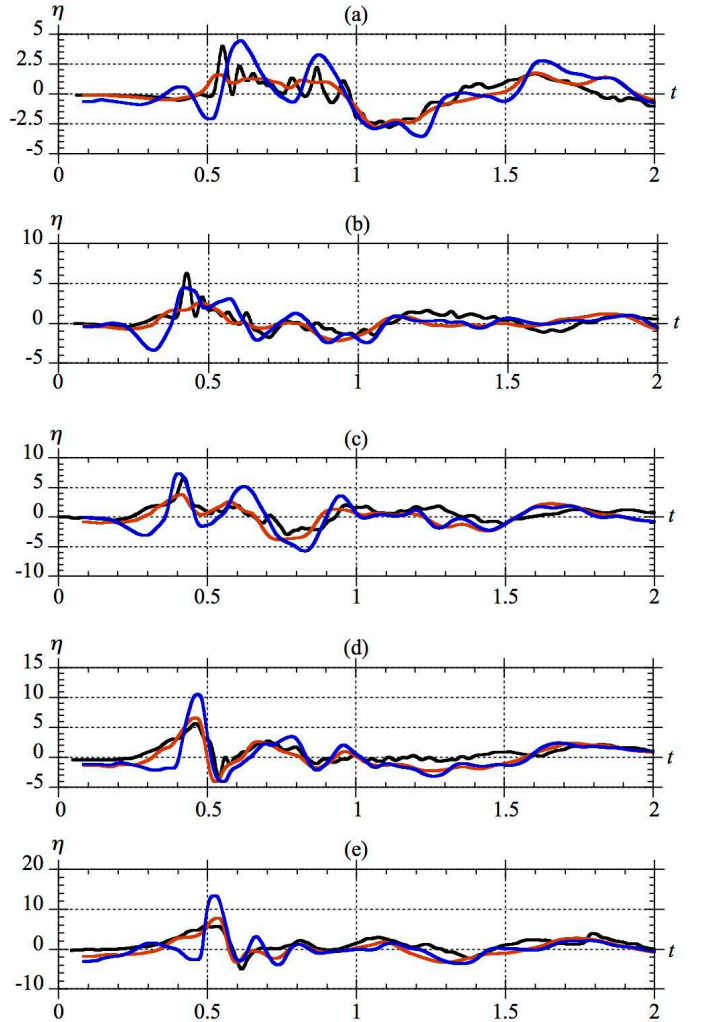

Fig. 6: Surface elevations (m) as a function of time (h), at some of the GPS buoys from N to S (Figs. 1), at: (a) North Iwate; (b) Central Iwate; (c) South Iwate; (d) North Miyagi; (e) Central Miyagi. Each panel compares observations (black) to computations for the : UCSB (M9) source (blue) and UA (M8.8) source (red).

Surface elevation at coastal GPS buoys

Fig. 6 compares surface elevations simulated at some GPS buoys with the UCSB and UA sources, to observations. Overall, the agreement is good for both sources. Although neither source matches the data as well
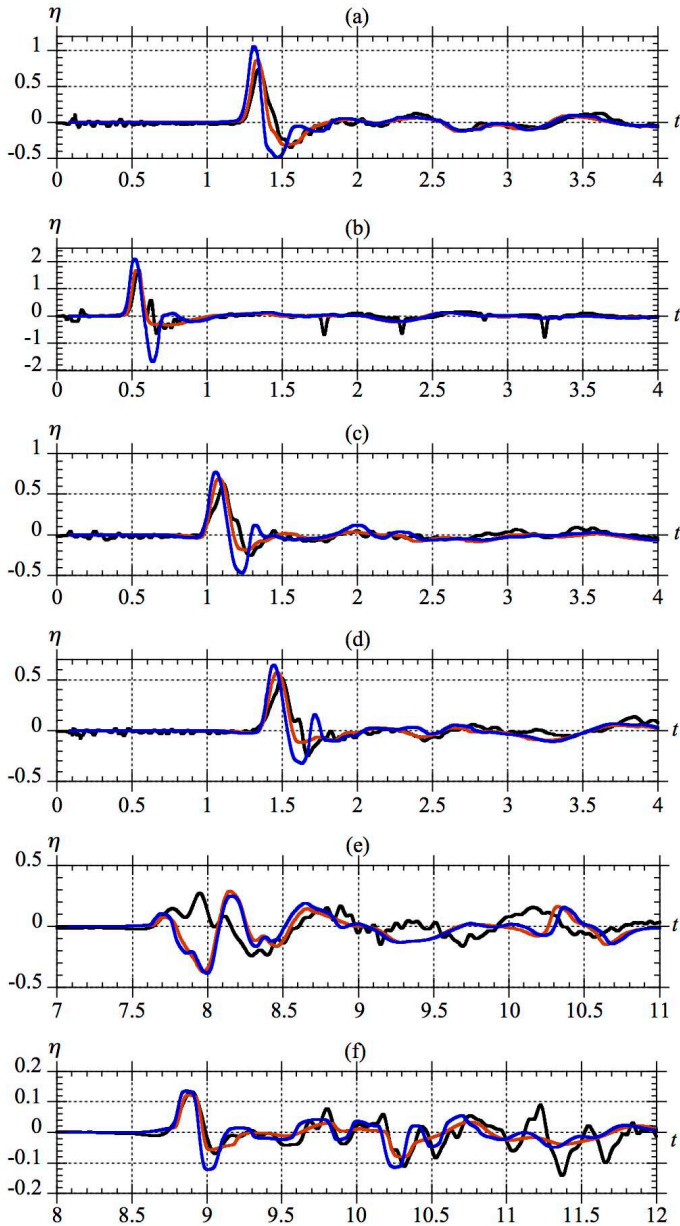
Fig. 7: Surface elevation (m) as a function of time (h) at DART buoys (Fig. 2) #: (a) 21413; (b) 21418; (c) 21401; (d) 21419; (e) 51407 (+6.6 min); (f) 46404 (+7.2 min). Comparison between observations (black) and computations with FUNWAVE-TVD using the : UCSB source (blue); and the UA source (red).

for the first 3 northern buoys (a-c), than further south (d-e), results of the UA source seem in better agreement with observations than those of the UCSB source, when considering the whole waveform. Note that our findings for the UCSB source results are somewhat similar to those of Yamazaki et al. (2011b), which show generally good agreement with the buoy data, but for some stations (i.e., North and Central Miyagi) their simulations underpredict the observed amplitude, and for others (i.e., South Miyagi, not shown here, which they refer to as the Fukushima GPS station) they overpredict the initial amplitude.

Trans-Pacific propagation and dispersive effects

Simulation were run for 24 hours of tsunami propagation, in order for waves to reach the most distant DART buoys and the South American coastline. Figs. 7, a-d shows a comparison of computed surface elevations with the UCSB and UA sources, and measurements at the four DART buoys closest to Japan (i.e., No. 21413, 21418, 21401, and 21419; Fig. 2). Overall, results for both the UCSB and UA sources agree well with observations. The UCSB source, however, consistently overpredicts the leading wave crest elevation at each location and, more notably, overpredicts the amplitude of the leading wave troughs. Both the UA and UCSB sources predict that the wave arrives slightly sooner than seen in observations, but this is more pronounced for the UCSB source. Figs. 7, e,f similarly show a comparison of computed and measured surface elevations at two distant DART buoys, in Hawaii and of of Oregon (i.e., No. 51407, 46404; Fig. 2). Similar to Yamazaki et al. (2011b), we find that the tsunami arrives earlier than observed (about 7 mins). Hence, to allow for an easier comparison, slight time shifts have been added to simulations in the figure, in order to synchronize the first elevation wave with that observed. These only represent about 1.5% of the tsunami propagation time and can be explained in part by a combination of grid and bathymetric resolution effects, as well as slight errors in the source location and triggering. Additional systematic errors on propagation times could results from the fact that the Earth is not perfectly spherical. [For these simulations, we assumed an earth radius of 6,371 km.] The predicted surface elevations at distant DART buoys generally agree reasonably well with observations and, at buoy (f), the UA source matches the leading wave much better than the UCSB source.

Figure 8, a shows the envelope of computed maximum wave elevation (for the UCSB source). We see, the tsunami energy propagates across the ocean in some preferential directions, associated with both the source characteristics and the ocean bathymetry, in which ridges may cause wave-guiding effects. This is particularly clear for the eastward propagation towards Northern California, around 40° N; large wave oscillations (nearly 4 m trough to crest) and damage were indeed observed at this latitude in Crescent City, CA. Frequency dispersion effects on this propagation are assessed by re-running these simulations without dispersion terms in FUNWAVE-TVD's equations (i.e., in NSW mode). Figure 8, b shows a difference plot between results with and without dispersion. As could be expected from the short propagation distances and the coarse grid resolution, little dispersive effects can be seen in the near field, close to Japan. In the far-field, however, non-negligible differences with NSW results, of more than ±10 cm, can be seen in deep water, which may amount to 20-40% of the tsunami amplitude at some locations. This is on the same order of magnitude as that of dispersive effects reported by Ioualalen et al. (2007) for the 2004 Indian Ocean tsunami and justifies using a BM in the present case. A more detailed discussion and analysis of dispersive effects and their comparison to Coriolis force effects for the Tohoku 2011 event can be found in Kirby et al. (2012).

Runup and inundation

After 300 s of simulations in the regional grid, the tsunami is simulated for another 2 hours in the coastal grid. Both runup and inundation data are available from the field surveys. In order to accurately predict runup, however, particularly in the north along the Sanriku/Ria coast (39.5° and 40.25° N), which has a very complex topography that could greatly enhance it, one needs to use a much finer model grid than 250 m (perhaps down to 20-30 m resolution). This would also require using a better resolved bathymetry than the 500 m data set currently used. Hence, with the current grid resolution, we believe a comparison with inundation results is more realistic than runup, as inundation is predicted at the shoreline. This is done in Fig. 9, where computed inundations for both sources are
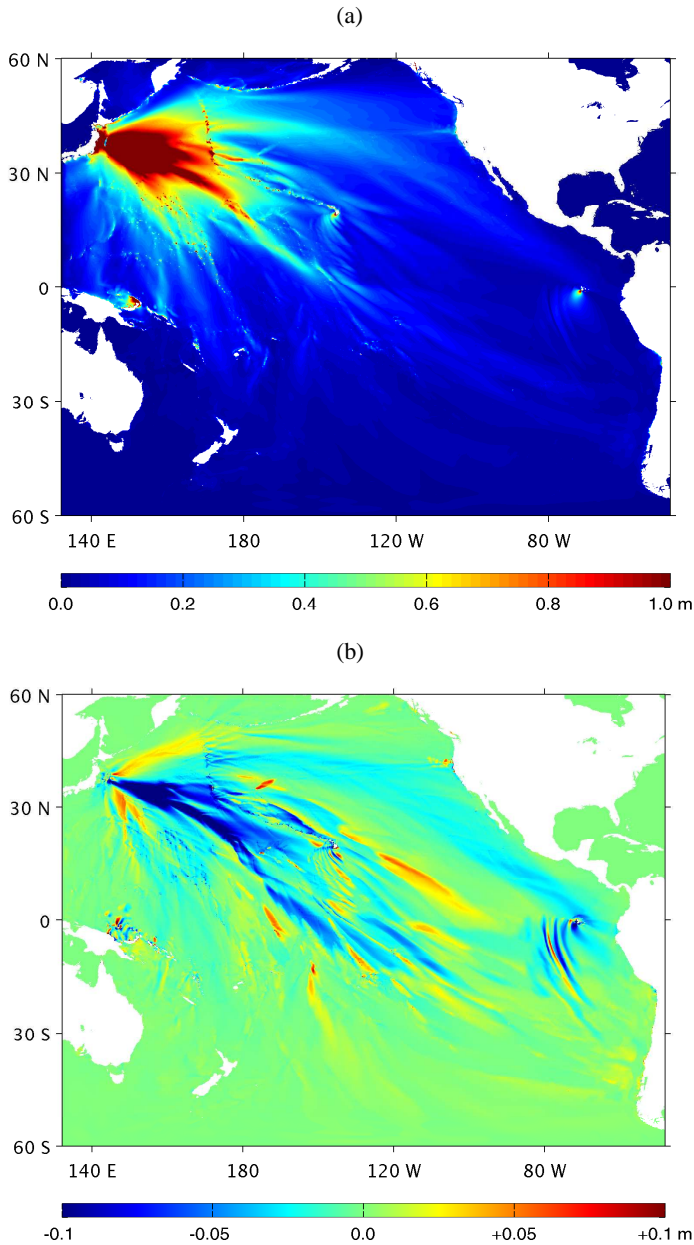
Fig. 8: (a) Maximum wave elevation computed with FUNWAVE-TVD in the spherical (4') Pacific grid for the UCSB source. (b) Difference between (a) and a (non-dispersive) NSW simulation of the same case.

directly compared to observed inundation values, north of 36° N. In this region, results for the UA source are found in good agreement with observations, except between 39.1° and 40.2° N, where these are significantly underpredicted in the model. By contrast, as already seen at some GPS and nearsore DART buoys, the UCSB source significantly overpredicts the observed inundation from 38.25° to 39.7° N (and thus the corresponding seafloor deformation offshore) and, like the UA source, underpredicts the inundation between 39.7° and 40.2° N, albeit by a smaller factor. Overall, based on these results, the UA source is seen to agree better with tsunami observations.

SUMMARY

We simulated tsunami generation propagation, near-field (coastal), and far-field impact of the Tohuku 2011 tsunami and compared results to field observations of surface elevation at DART buoys, GPS gage buoys, and runup and inundation along the most impacted coastal area of Japan (from 35°-41° N). Our BM model was initialized based on co-seismic tsunami sources developed from seismic (UCSB; Shao et al. (2011)) or GPS data (UA) inversion based on a detailed FEM of the subduction zone. Results showed that dispersive effects are negligible in the near-field, but may account for 20-40% of tsunami amplitude in deep water, hence justifying the use of a Boussinesq model. The sensitivity of results to three source triggering methods was assessed for the UCSB co-seismic source. Results justified using the 3rd more accurate and realistic method with a time dependent bottom boundary condition in NHWAVE, to compute the initial tsunami waveform.

Salient features of the observed tsunami far-field and coastal impact were well reproduced for both sources, but coastal impact was over- or under-estimated at some locations. Overall, however, results obtained for the UA source were found in better agreement with observations at nearshore GPS gages and DART buoys, and at some distant DART buoys, than those for the UCSB source. It was found that both sources accurately predicted inundation observations south of 38° N. To the north, results for the UA source were found in good agreement with observations, except between 39.7° and 40.2° N, where they were underpredicted. In addition to the complex coastline mentioned above, this is an area where the UA source may lack in tsunami generation, perhaps due to underpredicted seafloor deformations; but this could also be due to other phenomena not included in the co-seismic sources (e.g., splay faults, underwater landslides,...). In fact, there were early indications that Submarine Mass Failures (SMFs) may have been triggered in the Japan trench by the Tohuku-Oki M9 earthquake (Fujiwara et al., 2011). By contrast, the UCSB source significantly overpredicted observed inundations up to 39.7° N and, like the UA source, underpredicted inundation between 39.7° and 40.2° N, albeit by a smaller factor.

Overall, the UA source was thus found to agree better with tsunami observations, in both the near- and far-field, than those using the UCSB source, although it may need additional refinements to better explain observations between 39.7° and 40.2° N; these are currently in development and expected to be available in the near future.
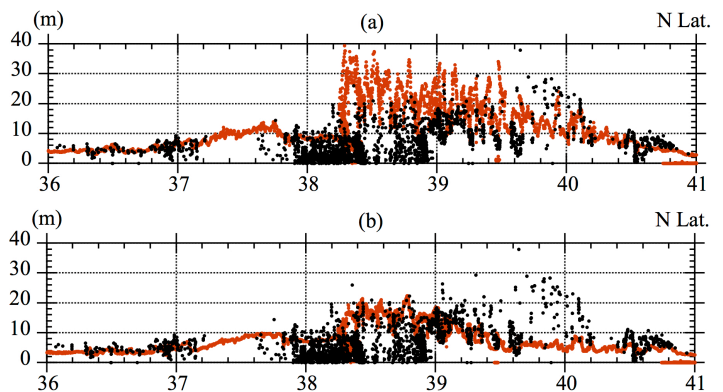

Fig. 9: Tsunami inundation measured (black dots) and computed (red) with: (a) M9 UCSB source; and (b) M8.8 UA source.

REFERENCES

Abaqus (2009). *Abaqus*. Dassault Systemes Simulia Corp., Providence, RI, 6.9-EF edition.

Ammon, C. J., Lay, T., Kanamori, H., and Cleveland, M. (2011). A rupture model of the great 2011 Tohoku earthquake. *Earth Planets Space*, (accepted):4 pp.

Chen, Q., Kirby, J. T., Dalrymple, R. A., Kennedy, A. B., and Chawla, A. (2000). Boussinesq modeling of wave transformation, breaking and runup. II: Two horizontal dimensions. *J. Waterway, Port, Coastal and Ocean Engrng.*, 126:48–56.

Chen, Q., Kirby, J. T., Dalrymple, R. A., Shi, F., and Thornton, E. B. (2003). Boussinesq modeling of longshore currents. *Journal of Geophysical Research*, 108(C11):3362.

Day, S. J., Watts, P., Grilli, S. T., and Kirby, J. (2005). Mechanical models of the 1975 kalapana, hawaii earthquake and tsunami. *Marine Geology*, 215(1-2):59–92.

DeMets, C., Gordon, R., and Argus, D. (1994). Effect of recent revisions to the geomagnetic reversal time scale on estimates of current plate motions. *Geophysical Research Letters*, 21:2191–2194.

Enet, F. and Grilli, S. T. (2007). Experimental study of tsunami generation by three-dimensional rigid underwater landslides. *Int. J. Num. Meth. Fluids*, 133:442–454.

Fujiwara, T., Kodaira, S., No, T., Kaiho, Y., Takahashi, N., and Kaneda, Y. (2011). Tohoku-Oki earthquake: Displacement reaching the trench axis. *Science*, 334:1240.

Geospatial Information Authority of Japan (2011). The 2011 off the Pacific coast of Tohoku Earthquake: Crustal Deformation and Fault Model (Preliminary). http://www.gsi.go.jp/cais/topic110313-index-e.html,2011.

Gica, E., Spillane, M., Titov, V., Chamberlin, C., and Newman, J. (2008). Development of the forecast propagation database for NOAA's Short-term Inundation Forecast for Tsunamis (SIFT). Technical report, NOAA Tech. Memo. OAR PMEL-139,89 pp.

Gonzalez, F. I., Milburn, H. M., Bernard, E. N., and Newman, J. C. (1998). Deep-ocean Assessment and Reporting of Tsunamis (DART): brief overview and status report. In *Proceedings of the International Workshop on Tsunami Disaster Mitigation*, Tokyo, Japan.

Grilli, S., Dubosq, S., Pophet, N., Prignon, Y., Kirby, J., and Shi, F. (2010). Numerical simulation and first-order hazard analysis of large co-seismic tsunamis generated in the puerto rico trench: near-field impact on the north shore of puerto rico and far-field impact on the us east coast. *Natural Hazards and Earth System Sciences*, 10:2109–2125.

Grilli, S., Harris, J., Tajalibakhsh, T., Masterlark, T., Kyriakopoulos, C., Kirby, J., and Shi, F. (2012). Numerical simulation of the 2011 tohoku tsunami based on a new transient fem co-seismic source: Comparison to far- and near-field observations. *Pure and Applied Geophysics*, (submitted):54pps.

Grilli, S., Ioualalen, M., Asavanant, J., Shi, F., Kirby, J., and Watts, P. (2007). Source constraints and model simulation of the December 26, 2004 Indian Ocean tsunami. *Journal of Waterway Port Coastal and Ocean Engineering*, 133(6):414–428.

Hughes, K., Masterlark, T., and Mooney, W. (2010). Poroelastic stress-coupling between the M9.2 2004 Sumatra-Andaman and M8.7 2005 Nias earthquakes. *Earth and Planetary Science Letters*, 293:289–299.

Ide, S., Baltay, A., and Beroza, G. (2011). Shallow dynamic overshoot and energetic deep rupture in the 2011 Mw 9.0 Tohoki-Oki earthquake. *Science*.

IOC/UNESCO (2011). Casualties by the earthquake and tsunami of March 11, 2011. *Bulletin No. 29 (9/30/2011), Intergovernmental Oceanographic Commission*.

Ioualalen, M., Asavanant, J., Kaewbanjak, N., Grilli, S., Kirby, J., and Watts, P. (2007). Modeling the 26th December 2004 Indian Ocean tsunami: Case study of impact in Thailand. *Journal of Geophysical Research*, 112(C07024).

Karlsson, J., Skelton, A., Sanden, M., Ioualalen, M., Kaewbanjak, N., andJ. Asavanant, N. P., and von Matern, A. (2009). Reconstructions of the coastal impact of the 2004 Indian Ocean tsunami in the Khao Lak area, Thailand. *Journal of Geophysical Research*, 114(C10023).

Kennedy, A. B., Chen, Q., Kirby, J. T., and Dalrymple, R. A. (2000). Boussinesq modeling of wave transformation, breaking, and run-up. I: 1D. *J. Waterway, Port, Coastal and Ocean Engrng.*, 126(1):39–47.

Kirby, J. T., Pophet, N., Shi, F., and Grilli, S. T. (2009). Basin scale tsunami propagation modeling using boussinesq models: Parallel implementation in spherical coordinates. *In Proc. WCCE-ECCE-TCCE Joint Conf. on Earthquake and Tsunami (Istanbul, Turkey, June 22-24)*, paper 100:(published on CD).

Kirby, J. T., Shi, F., Harris, J. C., and Grilli, S. T. (2012). Sensitivity analysis of trans-oceanic tsunami propagation to dispersive and Coriolis effects. *Ocean Modeling*, (in preparation):42 pp.

Kowalik, Z. and Murty, T. S. (1993). *Numerical modeling of ocean dynamics*. World Scientific Pub.

Lay, T., Ammon, C., Kanamori, H., Xue, L., and Kim, M. (2011a). Possible large near-trench slip during the 2011 Mw 9.0 off the Pacific coast of Tohoku Earthquake. *Earth Planets Space*, 63:687–692.

Lay, T., Yamazaki, Y., Ammon, C. J., Cheung, K. F., and Kanamori, H. (2011b). The great 2011 Earthquake off the Pacific coast of Tohoku (Mw 9.0): Comparison of deep-water tsunami signals with finite-fault rupture model predictions. *Earth Planets Space*, 63:797–801.

Ma, G., Shi, F., and Kirby, J. T. (2012). Shock-capturing non-hydrostatic model for fully dispersive surface wave processes. *Ocean Modeling*, 43-44:22–35.

Masterlark, T. (2003). Finite element model predictions of static deformation from dislocation sources in a subduction zone: Sensitivities to homogeneous, isotropic, poisson-solid, and half-space assumptions. *J. Geophys. Res.*, 108(B11):17pp.

Masterlark, T. and Hughes, K. (2008). The next generation of deformation models for the 2004 M9 Sumatra-Andaman Earthquake. *Geophysical Research Letters*, 35:5 pp.

Mori, N., Takahashi, T., and The 2011 Tohoku Earthquake Tsunami Joint Survey Group (2011a). Nationwide Post Event Survey and Analysis of the 2011 Tohoku Earthquake Tsunami. *Coastal Engineering Journal*, (submitted):37 pp.

Mori, N., Takahashi, T., Yasuda, T., and Yanagisawa, H. (2011b). Survey of 2011 Tohoku earthquake tsunami inundation and run-up. *Geophysical Research Letters*, 38(L00G14):6 pp.

Okada, Y. (1985). Surface deformation due to shear and tensile faults in a half space. *Bulletin of the Seismological Society of America*, 75(4):1135–1154.

Ozawa, S., Nishimura, T., Suito, H., Kobayashi, T., Tobita, M., and Imakiire, T. (2011). Coseismic and postseismic slip of the 2011 magnitude-9 Tohoku-Oki earthquake. *Nature*, 475(7356):373–376.

Pollitz, F., Bürgmann, R., and Banerjee, P. (2011). Geodetic slip model of the 2011 M9.0 Tohoku earthquake. *Geophysical Research Letters*, 38:L00G08.

Sato, M., Ishikawa, T., Ujirara, N., Yoshida, S., Fujita, M., Mochizuki, M., and Asada, A. (2011). Displacement above the hypocenter of the 2011 Tohoku-Oki Earthquake. *Science*, 332:1395.

Shao, G., Li, X., Ji, C., and Maeda, T. (2011). Focal mechanism and slip history of 2011 Mw 9.1 off the Pacific coast of Tohoku earthquake, constrained with teleseismic body and surface waves. *Earth Planets Space*, 63:559–564.

Shi, F., Kirby, J. T., Harris, J. C., Geiman, J. D., and Grilli, S. T. (2012). A high-order adaptive time-stepping TVD solver for Boussinesq modeling of breaking waves and coastal inundation. *Ocean Modeling*, 43-44:36–51.

Tappin, D., Watts, P., and Grilli, S. (2008). The Papua New Guinea tsunami of 1998: anatomy of a catastrophic event. *Natural Hazards and Earth System Sciences*, 8:243–266.

Tehranirad, B., Shi, F., Kirby, J. T., Harris, J. C., and Grilli, S. T. (2011). Tsunami benchmark results for fully nonlinear Boussinesq wave model FUNWAVE-TVD, Version 1.0. Technical report, No. CACR-11-02, Center for Applied Coastal Research, University of Delaware.

The 2011 Tohoku Earthquake Tsunami Joint Survey Group (2011). Nationwide field survey of the 2011 off the Pacific coast of Tohoku earthquake tsunami. *Journal of Japan Society of Civil Engineers*, 67(1):63–66.

Watts, P., Grilli, S. T., Kirby, J. T., Fryer, G. J., and Tappin, D. R. (2003). Landslide tsunami case studies using a Boussinesq model and a fully nonlinear tsunami generation model. *Natural Hazards and Earth System Sciences*, 3:391–402.

Wei, G., Kirby, J. T., Grilli, S. T., and Subramanya, R. (1995). A fully nonlinear Boussinesq model for surface waves. I. Highly nonlinear, unsteady waves. *Journal of Fluid Mechanics*, 294:71–92.

Yamazaki, Y., Lay, T., Cheung, K., Yue, H., and Kanamori, H. (2011a). Modeling near-field tsunami observations to improve finite fault slip models for the 11 March 2011 Tohoku earthquake. *Geophysical Research Letters*, 38.

Yamazaki, Y., Volker, R., Cheung, K. F., and Lay, T. (2011b). Modeling the 2011 Tohoku-oki Tsunami and its Impacts on Hawaii. In *Proceedings of OCEANS 2011. Waikoloa, HI, USA. 9 pp.*